Stretching of Free Chains Confined in Concave Brush-Coated Nanocylinders

ARTICLE *in* MACROMOLECULES · MARCH 2012

Impact Factor: 5.8 · DOI: 10.1021/ma202620z

4 AUTHORS:

Rong Wang
Nanjing University
39 PUBLICATIONS **313** CITATIONS
SEE PROFILE

Sergei Egorov
University of Virginia
91 PUBLICATIONS **1,953** CITATIONS
SEE PROFILE

Andrey Milchev
Bulgarian Academy of Sciences
237 PUBLICATIONS **4,457** CITATIONS
SEE PROFILE

Kurt Binder
Johannes Gutenberg-Universität Mainz
1,065 PUBLICATIONS **45,231** CITATIONS
SEE PROFILE

Macromolecules

Article

pubs.acs.org/Macromolecules

Stretching of Free Chains Confined in Concave Brush-Coated Nanocylinders

Rong Wang,[†,‡] Sergei A. Egorov,[†,§] Andrey Milchev,*[,†,⊥] and Kurt Binder[†]

[†]Institut für Physik, Johannes Gutenberg-Universität Mainz, Staudinger Weg 7, D-55099 Mainz, Germany

[‡]Department of Polymer Science and Engineering, State Key Laboratory of Coordination Chemistry, Nanjing National Laboratory of Microstructures, School of Chemistry and Chemical Engineering, Nanjing University, Nanjing 210093, China

[§]Department of Chemistry, University of Virginia, Charlottesville, Virginia 22901, United States

[⊥]Institute of Physical Chemistry, Bulgarian Academy of Sciences, 1113 Sofia, Bulgaria

ABSTRACT: The structure of a free flexible macromolecule confined in a cylindrical nanopore whose wall is coated by a polymer brush is studied by Monte Carlo simulation, varying the grafting density as well as the radius of the cylindrical pore. Because of this confinement, the free chain is stretched in axial direction; while for small grafting densities of the brush the end-to-end distance increases monotonously with decreasing pore radius, a nonmonotonic variation occurs for larger grafting densities. We show that this effect is due to strong interpenetration of the free chain and the brush chains; for very narrow pores a strong layering of cylindrical shells is found, and comparison with self-consistent field calculations (SCF) shows that the latter can predict the nonmonotonic variation in qualitative accord with the simulation. The robustness of the SCF approach is then used to demonstrate the occurrence of the observed "*penetration transition*" in a broader range of chain lengths and grafting densities.

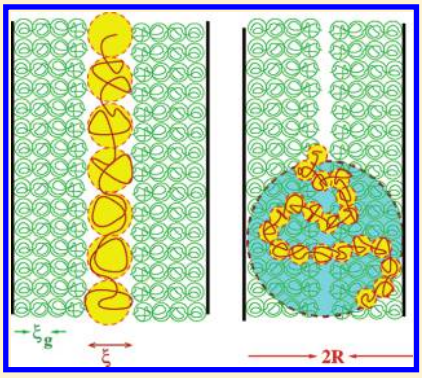

I. INTRODUCTION

Polymer brushes[1−7] are formed by grafting flexible macromolecules via a special end group on a nonadsorbing substrate surface, covering this substrate by a dense layer of chains stretched away from the substrate (under good solvent conditions). The thickness of these soft layers can be controlled by various external stimuli (temperature, pH-value of the solution, etc.) and polymer brushes on flat substrates allow numerous applications[8−11] and have been studied extensively (see, e.g., refs 11 and 12 for recent reviews).

Recently also brushes on concave surfaces in cylindrical surfaces have been considered[13−20] since such systems can possibly be used to control flow in nanocylindric channels,[21−25] to modify electroosmotic flow,[26,27] control transport of macromolecules through nanopores,[28−32] and to allow applications such as reversed phase[33] and size-exclusion[34,35] chromatography. Also in a biological context (biopolymer translocation through pores[36]) applications are conceivable.

While macromolecules confined in cylinders with bare repulsive walls have been considered for a long time,[37−44] the behavior of a macromolecule inside a brush-coated cylindrical pore has only been considered very recently.[20] Results obtained with self-consistent mean field (SCFT) calculations suggested a nonmonotonic dependence of the end-to-end distance of the confined macromolecule with the pore radius. This is in contrast to the behavior of polymers confined in tubes with bare repulsive walls where the variation is monotonic. Since the accuracy of mean field methods is doubtful in such a context (note also that the predicted minimum of the end-to-end distance occurs at a radius of about three lattice spacings of the SCFT scheme used[20]), it is rather desirable to clarify whether such nonmonotonic behavior also occurs, when one goes beyond mean field theory, and uses off-lattice models. Such a task can be performed by Monte Carlo simulation, as done in the present paper. Of course, the delicate structural changes of the macromolecule confined in such a cylindrical brush-coated pore have important implications on the transport of the polymer through the pore, but this latter problem will not be considered here. In section II, we describe the model that we study, and briefly comment on our simulation methods. Section III describes our simulation results, and section IV discusses the comparison with the SCFT results. Section V then summarizes our conclusions.

II. MODEL AND SIMULATION METHOD

We choose a cylinder with radius R and axial length L, orienting the cylinder axis along the z-direction, and applying periodic boundary conditions in the z-direction. The interaction between the wall and an effective monomer (irrespective of whether it belongs to the free chain or the grafted chains) is chosen to be purely repulsive, $U_w(r') = \varepsilon_w r'^{-9}$, where $r' = R - r$, $\varepsilon_w = 0.1$, r being the radial coordinate relative to the cylinder axis. In order to realize the conditions that the first monomer of

Received: December 3, 2011
Revised: February 4, 2012
Published: February 27, 2012

   dx.doi.org/10.1021/ma202620z | *Macromolecules* 2012, 45, 2580−2587

each grafted chain is tightly bound to the grafting surface, we choose a different potential for the first monomer, namely

$$U_{w,1}(r') = \varepsilon_w(r'^{-9} - fr'^{-9}), \quad f = 100 \tag{1}$$

We recall that the motivation for the choice of this particular form of the potential is the assumption of Lennard-Jones (6/12) interactions between any atom in the solid forming the wall and the effective monomers; integrating then these interactions over a (semi-infinite) half-space with a free (flat) surface, an interaction of the form eq 1 results. However, if one took such an argument literally, for the curved surface of a nanopore the actual potential clearly would be R-dependent. This complication is disregarded here, and we take eq 1 just as a generic model assumption, since we do not wish to address a specific system.

As is usually done, the arrangement of grafting sites is not chosen at random, but according to a regular pattern. The interaction between any pairs of monomers is chosen as a truncated and shifted Lennard-Jones (LJ) potential, while bonded monomers interact also with the standard FENE ("finitely extensible nonlinear elastic") potential. Thus, our potentials are of the same type as are standard for molecular dynamics simulations of polymer brushes.[5,12]

Specifically, we use

$$U_{LJ}(r) = \begin{cases} 4\varepsilon[(\sigma_{LJ}/r)^{12} - (\sigma_{LJ}/r)^6] + C, \\ \quad r < r_c = 2.2^{1/6}\sigma_{LJ} \\ 0, \quad r > r_c \end{cases} \tag{2}$$

Here $r = |\vec{r}_i - \vec{r}_j|$ is the distance between beads at positions $\vec{r}_i$ and $\vec{r}_j$. The constant C is chosen such that the potential $U_{LJ}(r)$ is continuous at the cutoff distance r_c. We use the LJ diameter $\sigma_{LJ} = 1$ as our length unit throughout. Similarly, we also take $\varepsilon = 1$ and Boltzmann's constant $k_B = 1$. The spring potential between two neighboring monomers then is

$$U_{FENE}(r) = \begin{cases} -\frac{1}{2}kr_0^2 \ln[1 - (r/r_0)^2], & r \le r_0 \\ \infty, & r > r_0 \end{cases} \tag{3}$$

with the usual choice $r_0 = 1.5$, $k = 20$. Remember that the total potential between two neighboring beads, $U_{LJ}(r) + U_{FENE}(r)$, has a minimum at $r_{min}^{(b)} \approx 0.96$, while the minimum of the LJ potential (acting between nonbonded monomers) occurs at $r_{min}^{(nb)} = 2^{1/6} \approx 1.12$. Because of this mismatch between $r_{min}^{(b)}$ and $r_{min}^{(nb)}$, this model has little tendency to form regularly ordered (crystalline) arrangements of the monomers at high density and/or low temperatures, respectively. In the present work, however, we wish to investigate the properties of the system only in the good solvent regime. Since for this model the Θ-temperature has been estimated to occur at $\Theta \approx 3.3$,[45,46] we work at $T = 4.0$, a case for which brush properties at flat substrates has already been studied.[47]

The simulations were carried out with standard Monte Carlo methods[48] but adopting several kinds of moves:[49] Local moves are done by choosing a position in the neighborhood. This neighborhood is a cube of linear dimension δ centered around the previous position of the chosen monomer. The magnitude of δ is chosen such that the average acceptance rate is close to 50%. For the grafted chains, also pivot rotations around the y-axis (an axis that is perpendicular to the grafting wall and goes through the position of a randomly chosen monomer i of a randomly chosen brush chain) are attempted. Choosing an angle φ uniformly distributed between 0 and 2π, the outer part of the grafted chain (i.e., the part of the chain from monomer i to N, if one labels the monomers consecutively from the grafted monomer to the free chain end) is rotated around this z-axis like a rigid object.[43,49] Of course, any such Monte Carlo move is only accepted if the standard Metropolis test is passed.[48,49] For the free chain, standard slithering snake moves are performed,[49] while no pivot moves were then attempted. Only a single choice of chain lengths is studied ($N = 8$ for the grafted chains, $N_f = 50$ for the free chains), which corresponds to the choice made in the previous[20] self-consistent field calculations. Of course, these chain lengths are extremely short, but one must consider that every bead of the simulated chains corresponds to $n \approx 3-5$ chemical monomers of a real polymer.[49] In our simulations, N local move attempts of a grafted chain are followed by 100 pivot move attempts, and one reptation move attempt is followed by N_f local move attempts for the free chain. We refer to this sequence of moves as "one Monte Carlo step". Typically 10^7 MCS were performed, and the first half of the run (5×10^6 MCS) is omitted to avoid any influence of the initial configuration.

III. SIMULATION RESULTS

We consider free chains with chain length $N_f = 50$ in brush-coated nanocylinders (choosing $N = 8$ for the brush chains) as a function of the pore radius R, for the four grafting densities $\sigma = 0.05$, 0.08, 0.10, and 0.12. The length of the cylinder then was chosen (remember that we work with a regular arrangement of grafting sites) $L = 35.77$, 38.89, 37.95, and 37.53, respectively. Here and in what follows, the monomer concentration in the tube is taken as particle number density.

Figure 1 presents the end-to-end distance of the free chain along the cylindrical axis as a function of the cylinder radius for

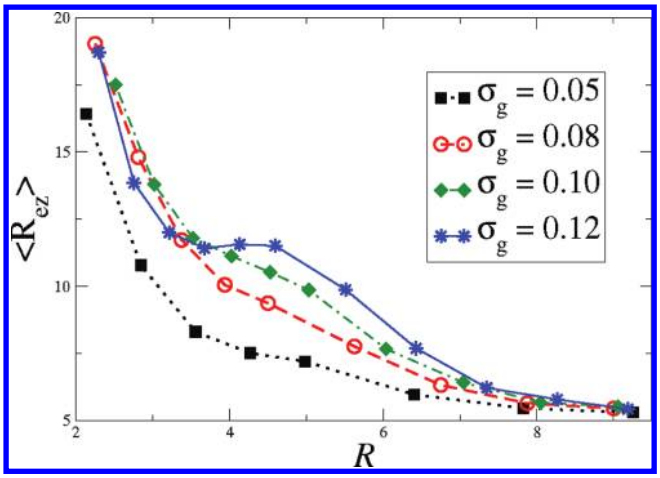

Figure 1. End to end distance of the free chain along the cylinder axis as a function of the cylinder radius R, for four grafting densities, as indicated.

the grafting densities that were studied. One can see that the end-to-end distance is almost constant when R is large. When the cylinder radius R decreases, the end-to-end distance of the free chain starts to increase, i.e. the chain stretches out along the cylinder axis. For the two smallest grafting densities ($\sigma = 0.05$ and 0.08) the variation of $\langle R_{ez}\rangle$ with R is monotonic, while for $\sigma = 0.10$ a flat plateau near $R = 4$ starts to develop, and for

dx.doi.org/10.1021/ma202620z | Macromolecules 2012, 45, 2580−2587

still larger σ (such as $\sigma = 0.12$) the variation is nonmonotonic. Note that the average end-to-end distance $\langle R_{ez} \rangle$ always is much smaller than the chosen cylinder length L, so there are no finite size effects due to the finite value of L to be expected.

Qualitatively, such a nonmonotonic variation of the end-to-end distance with the cylinder radius was predicted by self-consistent field calculations,[20] and hence, we confirm this result. The interpretation that can be given[20] is that for small grafting densities the grafted chains form a rather dense polymer layer at the cylinder wall, but near the cylinder axis there is a cylindrical region effectively free from the monomers of the grafted chains. The free chain then occupies the region of this inner cylinder, in which significant overlap with the monomers of the grafted chains can be avoided. The free chain then forms a rather long string of blobs in this region of the inner cylinder. However, when the cylinder radius is still smaller, the region near the cylinder axis then is also occupied by monomers of the grafted chains. Then there is no possibility for the free chain to avoid overlap with the grafted chains; and if the monomers of the grafted chains fill the cylinder more or less uniformly,[16,17] for entropic reasons it becomes advantageous for the free chain to form a string of blobs which have a radius comparable to the full cylinder radius. One might call appropriately the observed phenomenon, which is driven by osmotic pressure inside the brush coating, a *penetration transition*, given its universality and similarity to other cases of parameter-driven configurational changes in polymers. Indeed, one deals here with a *reversible* transformation in equilibrium that comes about due to free energy minimization. One should note, however, that this is a gradual rather than an abrupt transition and is, therefore, not a genuine "phase transition" in the sense of thermodynamics.

Regarding our methods of investigation, one should be aware that the self-consistent field results[20] may suffer from the mean field approximation inherent in the theory, and moreover, they were based on a rather crude discretization (using a lattice spacing of unity even though cylinder radii down to $R = 2$ were considered). Thus, it is of significant interest that the present off-lattice Monte Carlo simulations confirm this finding.

An advantage of the simulation, of course, is that very detailed information on the chain conformations can be extracted. Figure 2 therefore correlates typical snapshot pictures of the chain conformation at various conditions with the behavior of the end-to-end distance. Compare, e.g., the snapshots at $R = 3.6$ and $R = 6.4$: The projections on the *xy*-plane are rather similar in both cases, filling an almost circular region of a diameter of about 6. For the smaller value of R, this diameter is almost as large as $2R$, i.e., the free chain occupies space everywhere in the tube, while for the large value of R, D is much less than $2R$, so indeed the chain then avoids overlap with the brush chains to a large extent. For the largest value of R, the *xz*- and *xy*-projections of the free chain are already rather similar: now there is so much space available that the anisotropy of the conformation gets greatly reduced, and a crossover to the structure of a free unconfined chain in a solution occurs. In the regime of intermediate R, where the end-to-end distance depends most strongly on the grafting density, one notes also a corresponding effect on the radial distribution (Figure 3).

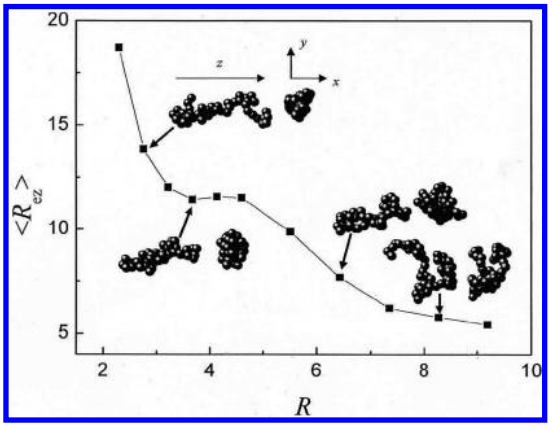

Figure 2. End to end distance of the free chain plotted vs R for $\sigma = 0.12$. The insert snapshots show typical conformations of the free chain showing projections on the *xz*-plane containing hence the axis of the cylinder (left) and on the perpendicular *xy*-plane (right).

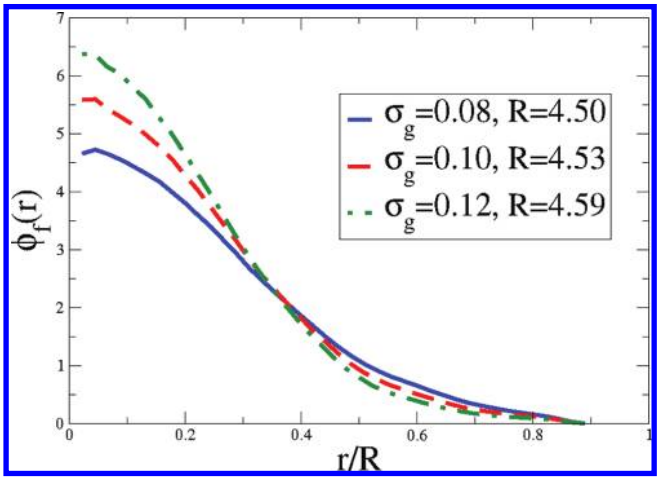

Figure 3. Radial distribution function $\phi_f(r)$ vs r/R of the free chain in the brush coated cylinder at three grafting densities for comparable values of R (the values of R slightly differ because of the requirement of putting a regular arrangement of grafting sites on the cylindrical surface at given grafting density). Note that with increasing σ the half width of the distributions decrease, consistent with the increase of $\langle R_{ez} \rangle$. The normalization has been chosen as $\pi \int_0^R \phi_f(r) r \, dr \, N_f = 50$.

A subtle aspect of the behavior shown in Figures 1, 2 is the fact that the total monomer concentration (that is, the number of particles per unit volume) in the cylinder varies from almost dilute ($c = 0.1$) to melt conditions ($c = 1.0$), see Figure 4. So, while for large R (where the concentration is small) the free chain will almost exhibit self-avoiding walk statistics ($\langle R_{ez} \rangle \propto N_f^{\nu}$ with $\nu \approx {}^3/_5$), for small R all correlations due to excluded volume are screened, and instead the monomers of the free chain and of the grafted chains are expected to share the available volume, as it happens in a typical polymer melt. However, the dense packing of monomers will lead to a considerable slowing down of the chain motions, and ultimately glassy freezing in of the free chain in the brush may be expected. However, molecular dynamics methods[16−18] would be more appropriate to study such aspects of the problem than Monte Carlo simulation, and hence we do not elaborate on this aspect further here.

To study the interpenetration of the free chain and the brush chains in more detail, we focus on the radial density profiles of the monomers (Figure 5). When the radius of the cylinder is very small, such as $R = 2.76$, the grafted chains show a very pronounced layering effect: actually there occur then three

dx.doi.org/10.1021/ma202620z | *Macromolecules* 2012, 45, 2580−2587

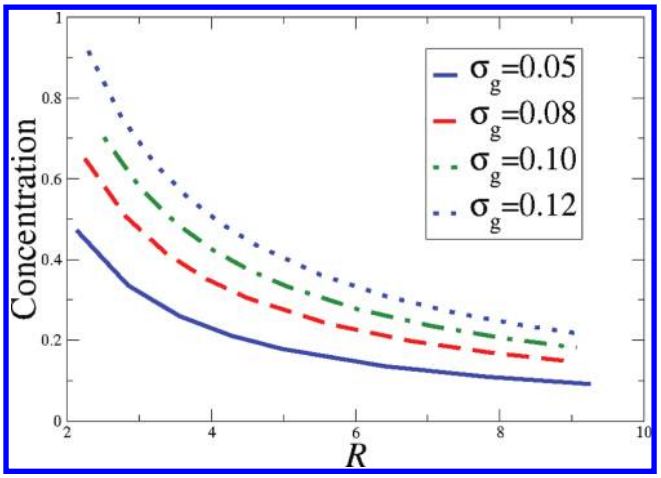

Figure 4. Total monomer concentration of the model (grafted chains plus one free chain) as a function of the cylinder radius R for the different grafting densities σ_g studied, as indicated. Here the concentration is normalized on the number of monomers per unit volume in the pore (remember the choice of length with $\sigma_{LJ} = 1$ for this model).

pronounced density maxima, for $r = 0$ (the cylinder axis), near $r = 1$ and near $r = 2$, respectively. It is remarkable that also the density distribution of the monomers of the free chain exhibits peaks at the same locations: the monomers of the free chain are incorporated into the layered structure enforced by this strong cylindrical confinement in a "democratic" fashion, together with the monomers of the grafted chains. For $R = 3.68$, on the other hand, the density distribution of the grafted monomers near the cylinder axis is almost flat, the maxima at $r = 0$ and near $r = 1$ are no longer clearly distinguished, while near $r = 2$ and $r = 3$ well-developed peaks do occur. $\phi_f(r)$ now is clearly largest in the center, although it still extends throughout the pore. For $R = 4.59$, however, $\phi_f(r \geq 2.5) \approx 0$, and while there is still considerable overlap of $\phi_f(r)$ with $\phi(r)$, the free chain now is confined near the cylinder axis.This segregation continues for larger R: even for $R = 8.27$ the monomer density of the grafted chains exhibits two pronounced layering peaks close to the wall, but only in an intermediate regime of r, $3 \leq r \leq 4$, there is still a bit of overlap between $\phi_g(r)$ and $\phi_f(r)$.

To quantify the overlap, we define the quantity

$$\varphi_{fg} = \int_0^\infty \varphi_g(r)\varphi_f(r) r\, dr / \int_0^\infty \varphi_f(r) r\, dr \quad (4)$$

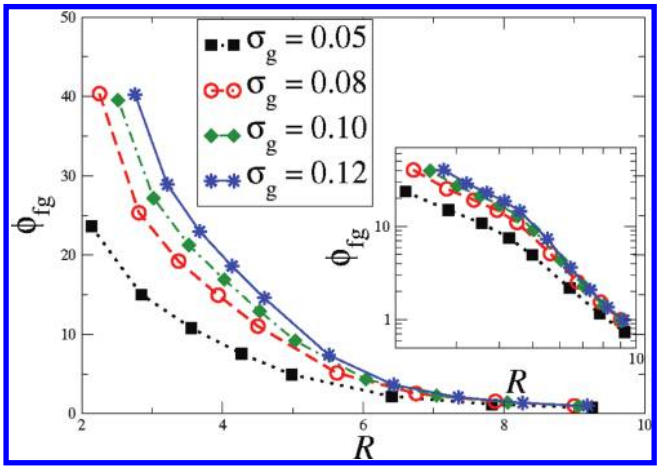

Figure 6. Overlap ϕ_{fg} between the monomer density distributions of the free chain and the grafted chains plotted vs R for several choices of σ_g, as indicated. Inset shows the same data on a log–log plot.

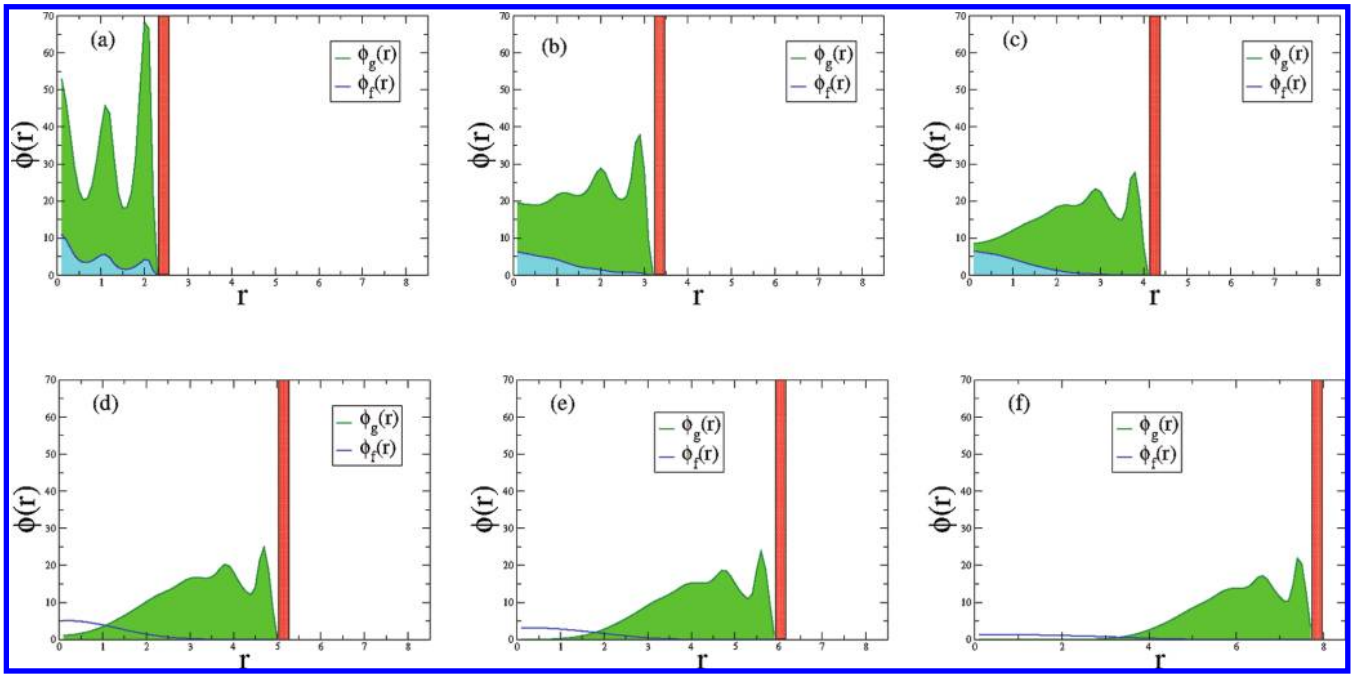

Figure 5. Radial density distribution of the monomers of the grafted chains $\phi_g(r)$, and of the free chain $\phi_f(r)$, plotted as a function of the distance r from the cylinder axis at grafting density $\sigma = 0.12$ and various choices of R: $R = 2.76$ (a), 3.68 (b), 4.59 (c), 5.51 (d), 6.43 (e) and 8.27 (f). The tube wall is also indicated. Note that normalizations have been chosen such that $2\pi\int_0^R \phi_g(r) r\, dr = N_g$, the total number of monomers in grafted chains in the system, and $2\pi\int_0^R \phi_f(r) r\, dr = N_f = 50$, the total number of monomers in the free chain.

dx.doi.org/10.1021/ma202620z | Macromolecules 2012, 45, 2580–2587

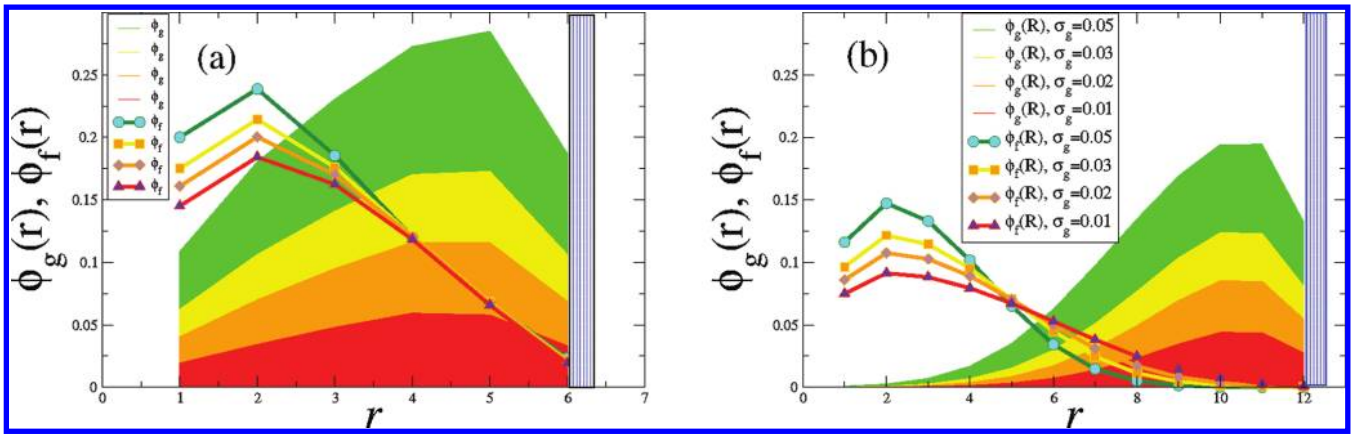

Figure 7. Monomer radial density profiles $\rho_g(r)$ and $\rho_f(r)$ of grafted (g) and free (f) chains for the case $N_f = 200$, $N = 16$, $R = 6$ (a), and $R = 12$ (b). In each case, four grafting densities are shown, $\sigma_g = 0.01$, 0.02, 0.03, and 0.05, as indicated in part a. Note that densities are defined at integer values of r only, and the boundary condition at $r = 0$, $n_g(0) = n_f(0) = 0$ has the consequence that the maximum of $\rho_f(r)$ occurs at $r = 2$ rather than at $r = 1$ (in contrast to what one expects from the continuum calculations, cf. Figure 3 and 5). Straight lines connecting points at integer values of r are guides to the eye only. Vertical bars beyond $R = 12$ (a) and $R = 6$ (b) indicate the confining cylindrical wall.

This quantity is plotted in Figure 6.[50] Again the behavior of the overlap indicates clearly two regimes with different slopes on the log–log plot, as in ref 20.

IV. COMPARISON WITH SELF-CONSISTENT FIELD RESULTS

The advantage of the self-consistent field theory (SCFT) is that it easily allows a generalization to longer chain lengths of both grafted chains (N) and of free chains (N_f), which would be more difficult to consider via Monte Carlo simulation. On the other hand, there are two approximations made, namely (i) the mean-field approximation inherent in all formulations of SCFT[3,51] (ii) The spatial discretization in terms of a cylindrical lattice. The latter leads to a somewhat different normalization of local densities than in the continuum, which we discuss first.

In the continuum, the grafted chains are localized in a volume $V_g = \pi R^2 L$, and the total number of monomers of grafted chains in the system is $\mathcal{N}_g = 2\pi RL\sigma_g N$, remembering that the grafting density σ_g refers to the surface $2\pi RL$ of the confining cylinder. The average monomer density due to grafted chains in the cylinders is

$$\bar{\rho}_g = \mathcal{N}_g/V_g = 2\sigma N/R \tag{5}$$

Introducing then a local density $\rho_g(r,z)$ per unit volume (z is the coordinate along the cylinder axis) we also have

$$\bar{\rho}_g = V_g^{-1} 2\pi \int_0^R r\,\mathrm{d}r \int_0^L \mathrm{d}z\, \rho_g(r,z) \approx (2/R^2) \int_0^R \rho_g(r) r\,\mathrm{d}r \tag{6}$$

where in the last step we have assumed that $\rho_g(r,z)$ is independent of z, $\rho_g(r,z) \approx \rho_g(r)$, even if a free chain is present in part of the cylinder. The free chain is present only in a piece of the cylinder of length R_{ez} with $V_f = \pi R^2 R_{ez}$, R_{ez} being the end-to-end distance of the chain, from $z = z_1$ to $z = z_1 + R_{ez}$. In this region, we have an average density of monomers of the free chain given by

$$\bar{\rho}_f = N_f/(\pi R^2 R_{ez}) \tag{7}$$

which alternatively can be written as an average over the local density $\rho_f(r,z)$

$$\bar{\rho}_f = V_f^{-1} 2\pi \int_{z_1}^{z_1+R_{ez}} \mathrm{d}z \int_0^R \rho_f(z,r) r\,\mathrm{d}r \approx \frac{2}{R^2} \int_0^R \rho_f(r) r\,\mathrm{d}r \tag{8}$$

Here again the approximation is made that $\rho_f(z,r)$ does not depend on z, in the regime $z_1 \le z \le z_1 + R_{ez}$, while outside of this regime $\rho_f(z,r) = 0$, of course. This approximation is certainly doubtful near the chain ends of the free chain, of course, but then $\rho_f(r)$ still can be interpreted as an average along z, $R_{ez}^{-1} \int_{z1}^{z1+Rez} \mathrm{d}z\, \rho_f(r,z)$. In fact, data shown in Figures 3 and 5 have to be understood in this way. With these normalizations, $\rho_g(r)$ and $\rho_f(r)$ can be compared on an absolute scale, denoting both numbers of monomeric units per volume element.

These considerations can be carried over the SCFT treatment, where one introduces planes equidistant perpendicular to the z-axis ($\Delta z = 1$), and in each plane one has concentric circles around the z-axis, with radii $r = 1, 2, 3, R$.[52] The number of occupied sites at each circle (integrated over z) is defined as $2\pi n(r)$. Thus, the total number of monomers due to grafted chains in the system is

$$\mathcal{N}_g = 2\pi \sum_{r=1}^{R} n_g(r) = 2\pi RL\sigma_g N \tag{9}$$

and hence the local density of monomers from grafted chains and per length Δl=1 along the circle of radius r and per $\Delta z = 1$ simply is

$$\rho_g(r) = n_g(r)/(rL) \tag{10}$$

since the area of the cylinder surface at radius r is $2\pi rL$ (and the factor 2π has been written explicitly in eq 9. The density $\rho_g(r)$ of eq 10 becomes identical to $\rho_g(r)$ as used in eq 6 in the continuum limit (when $r \gg \Delta r = 1$ and $z \gg \Delta z = 1$ is considered).

dx.doi.org/10.1021/ma202620z | Macromolecules 2012, 45, 2580–2587

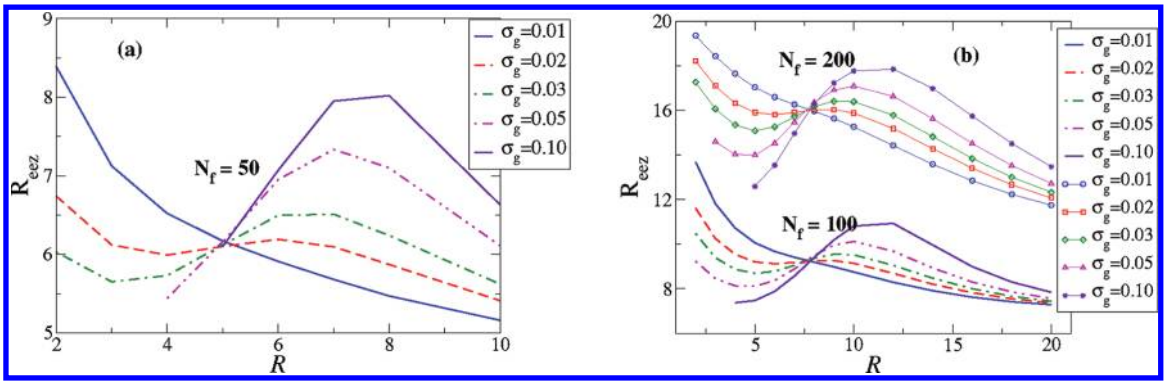

Figure 8. SCFT results for the end-to-end distance $\langle R_{ez}\rangle$ of a free chain along the cylinder axis plotted vs the cylinder radius R, for several grafting densities (as indicated) and the cases (a) $N = 8$, $N_f = 50$, and (b) $N = 16$, $N_f = 100$, and $N_f = 200$. A single intersection point is observed at $R^{is} \approx 5.01R$ (a), and $R^{is} \approx 7.74R$ (b).

For the free chains, we have analogously

$$\mathcal{N}_f = 2\pi \sum_{r=1}^{R} n_f(r),\ \rho_f(r) = n_f(r)/(rR_{ez}) \tag{11}$$

While along the z-axis monomers of grafted chains occur over the full length L, monomers of the free chain occur only over a distance R_{ez}, the end-to-end distance in z-direction. Equation 11 directly corresponds to $\rho_f(r)$ as considered in the continuum theory (eq 8).

Now SCFT provides a numerical recursion scheme,[20,52] from which $n_g(r,z)$, $n_f(r,z)$, the corresponding monomer numbers on a circle at radius r in plane z, can be constructed.[20,52] Of course, one has the sum rules $n_f(r) = \sum_z n_f(r,z)$ and $n_g(r) = \sum_z n_g(r,z)$. Indeed the calculation shows that the z-dependence of $n_g(r,z)$ can be neglected completely, and also the z-dependence of $n_f(r,z)$ is not important in the regime of z in between the two chain ends, as assumed above. Figure 7 shows typical results for $\rho_g(r)$ and $\rho_f(r)$ as obtained from the SCFT calculations. Recall that in this figure the normalization of densities is such that $\rho_g(r) + \rho_f(r) = \rho_{tot}(r)$, so one sees that in the case of strong interpenetration ($R = 6$, Figure 7b) the total density $\rho_{tot}(r)$ varies less than the individual contributions $\rho_g(r)$, $\rho_f(r)$, and reaches a broad maximum ($\rho_{tot}^{max} \approx 0.4$) in between $r = 2$ and $r = 4$. Note that $\rho_f(r \geq 3)$ is almost independent of σ_g: it would cost too much entropy for the free chain to use only the space close to the cylinder axis, and hence interpenetration between the brush and the free chain is inevitable. For $R = 12$, on the other hand, grafted chains do not extend toward the region of the cylinder axis. Of course, the lattice SCFT model cannot reveal details of the simulation of the continuum model, such as the pronounced layering of the local density (Figure 5). But the bonus of the lattice SCFT model is that much longer chains can be handled, and a comprehensive variation of parameters is much easier. Thus, we can make sure that the nonmonotonic variation of $\langle R_{ez}\rangle$ with R (for large enough grafting densities) is a generic effect; see Figure 8. Note that in Figure 8 data are only available at integer R (highlighted by points which are connected by straight lines to guide the eye). Because of this discretization, we cannot say with certainty whether or not SCFT strictly predicts a unique intersection point for different σ_g (as the curves seem to suggest). At present, we are not aware of a convincing theoretical argument as to why such a single intersection point should exist either. In any case, the location of this apparent intersection can be taken as an estimate for the location of the "penetration transition" where the blobs of the free chain penetrate into the brush.

Finally, Figure 9 presents a log–log plot of the overlap (defined in analogy to eq 4) vs R. Note that for a given choice

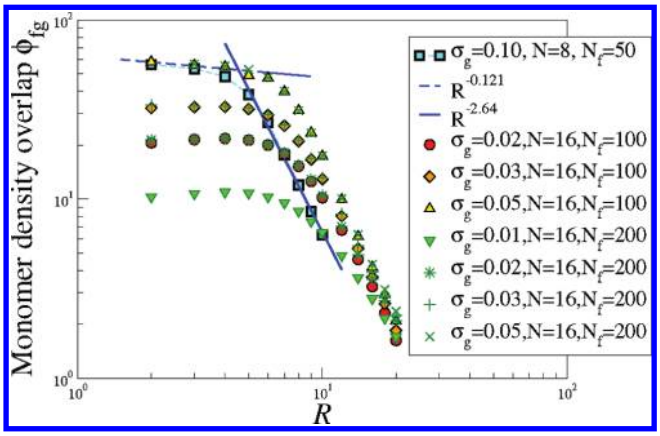

Figure 9. Overlap ϕ_{fg} (eq 4) between the density profiles of free and grafted chains, shown as log–log plot vs R. Various choices of N, N_f, and σ_g are included.

of σ_g and N it does not matter how large N_f is chosen: if we take $N_f = 200$ instead of $N_f = 100$, R_{ez} is twice as large, of course. But $\rho_f(r)$ does not change, due to the homogeneity of $\rho_f(r,z)$ with respect to z (in the regime $z_1 \leq z \leq z_{Nf} = z_1 + R_{ez}$). Thus, such data sets superimpose precisely. We also very clearly recognize that there always occur two regimes: (i) a regime of significant overlap, almost independent of R. The value of the overlap in this regime is roughly proportional to σ_g, while (ii) for large R, where the overlap is small, the overlap is almost independent of σ_g. The overlap for large R decays with an apparent power law, but we do not have a theoretical explanation for this behavior. The value of R where the onset of this power law occurs roughly agrees with the position where the R_{ez} vs R curves for different σ_g intersect. This crossover occurs at larger R when N increases but does not depend on N_f.

V. CONCLUSIONS

In this paper, the conformation of flexible polymer chains confined in nanotubes coated with polymer brushes formed from very short chains has been studied by Monte Carlo simulations and by numerical lattice SCFT calculations. We have shown that there is a delicate interplay between a possible

dx.doi.org/10.1021/ma202620z | Macromolecules 2012, 45, 2580–2587

interpenetration of the free chain with the brush chains and the axial stretching of the free chains, for the case of good solvent conditions that is studied throughout. For very narrow nanotubes, the monomers arrange in the tube in concentric cylindrical shells, reminiscent of the layering of particles in dense fluids adjacent to hard walls; these shells are shared by monomers of the free and grafted chains. This layering effect can be described by off-lattice models. The lattice SCF theory (or other lattice models where polymers are described by self-avoiding walks on the simple cubic lattice) is not suited for a description of this effect. However, the SCFT calculations provide a rather reliable description for the dependence of the end-to-end distance of the free chains and the overlap between free and grafted chains. As the radius of the nanotube decreases, first the free chain gets more and more stretched. Then a 'penetration' transition takes place when the free energy cost of further confinement gets too unfavorable in comparison with the free energy cost of the strong interpenetration.

In our previous work,[20] we have interpreted this effect qualitatively in terms of a blob picture, however, one should not take the blob picture too seriously. One can see from the present numerical results, that the overlap between free and grafted chains starts already when the free chain is only weakly confined and its conformation is only weakly perturbed, cf. Figure 2, in comparison with the conformation of a free chain in solution. The snapshot pictures shown in Figure 2 clearly indicate that one must not take the description of confined polymers in terms of linear cigar-like strings of blobs literally. Also the numerical lattice SCFT results presented in section IV demonstrates that the behavior of the system changes rather gradually when parameters such as pore diameter, grafting density, chain length of the grafted chains, etc. are varied, even though this method does not give as many details on the chain conformation as the simulation.

Of course, there are still open questions regarding the possible effects of solvent quality variation, chemical mismatch between the grafted and free chains, chain stiffness, etc. The dynamics of the confined free chain is a problem that could be of interest for applications too. Therefore, we hope that the present work will stimulate further research in this area.

AUTHOR INFORMATION

Notes

The authors declare no competing financial interest.

ACKNOWLEDGMENTS

R.W. and S.A.E. acknowledge partial support both by the Alexander von Humboldt foundation and by the Deutsche Forschungsgemeinschaft (DFG) under grant No SFB625/A3. A.M. and K.B. acknowledge the support from the DFG under Grant No. Bi 314/23. S.A.E is grateful to Prof. F. Leermakers for his sharing and help with using the software package *sfbox* which was employed for the calculations presented in section IV. R.W. is indebted to Dr. P. Virnau and Dr. H.-P. Hsu for useful discussions, and thanks the National Natural Science Foundation of China (Grant Nos 20874046, 21074053) and National Basic Research Program of China (Grant No 2010CB923303) for financial support and thanks to the Institut für Physik at the Johannes Gutenberg Universität Mainz for its hospitality.

REFERENCES

(1) Alexander, S. *J. Phys. (Paris)* **1977**, *38*, 983.
(2) De Gennes, P. G. *Macromolecules* **1980**, *13*, 1069.
(3) Milner, S. T. *Science* **1991**, *251*, 905.
(4) Halperin, A.; Tirrell, M.; Lodge, T. P. *Adv. Polym. Sci.* **1992**, *100*, 33.
(5) Grest, G. S.; Murat, M. In *Monte Carlo and Molecular Dynamics Simulations in Polymer Science*; Binder, K., Ed.; Oxford Univ. Press: New York, 2005.
(6) Szleifer, I.; Carignano, M. A. *Adv. Chem. Phys.* **1996**, *94*, 165.
(7) Leger, L.; Raphael, E.; Hervet, H. *Adv. Polym. Sci.* **1999**, *138*, 185.
(8) Napper., D. H,. *Polymeric Stabilization of Colloidal Dispersions*; Academic: London, 1983.
(9) Klein, J. *Annu. Rev. Mater. Sci.* **1996**, *26*, 581.
(10) Mansky, P.; Liu, Y.; Huang, T. P.; Russell, T. P.; Hawker, C. *Science* **1997**, *275*, 1485.
(11) Advincula, R. C.; Brittain, W. J.; Caster, K. C.; Rühe, J. (Eds.) *Polymer Brushes*: Wiley-VCH: Weinheim, Germany, 2004.
(12) Binder, K.; Kreer, T.; Milchev, A. *Soft Matter* **2011**, *7*, 7159.
(13) Sevick, E. M. *Macromolecules* **1996**, *29*, 6952.
(14) Manghi, M.; Aubouy, M.; Gay, C.; Ligoure, C. *Eur. Phys. J. E., Soft Matter, Biol. Phys.* **2001**, *5*, 519.
(15) (a) Viduna, D.; Limpouchova, Z.; Prochazka, K. *J. Chem. Phys.* **2001**, *115*, 7309. (b) *Macromol. Theory Simul.* **2001**, *10*, 165.
(16) Dimitrov, D. I.; Milchev, A.; Binder, K. *J. Chem. Phys.* **2006**, *125*, 034905.
(17) Dimitrov, D. I.; Milchev, A.; Binder, K.; Heermann, D. I. *Macromol. Theory Simul.* **2006**, *15*, 573.
(18) Dimitrov, D. I.; Milchev, A.; Binder, K. *Macromol. Symp.* **2007**, *252*, 47.
(19) Koutsioukas, A. G.; Spiliopoulos, N.; Anastassopoulos, D. L.; Vradis, A. A.; Toprakcioglu, C. *J. Chem. Phys.* **2009**, *131*, 044901.
(20) Egorov, S. A.; Milchev, A.; Klushin, L.; Binder, K. *Soft Matter* **2011**, *7*, 5669.
(21) Adiga, S. P.; Brenner, D. W. *Nano Lett.* **2005**, *5*, 2509.
(22) Adiga, S. P.; Brenner, D. W. *Macromolecules* **2007**, *40*, 1342.
(23) Dimitrov, D. I.; Klushin, L. I.; Milchev, A.; Binder, L. *Phys. Fluids* **2008**, *20*, 092107.
(24) Dimitrov., D. I.; Milchev, A.; Binder, K. *Ann. N.Y. Acad. Sci.* **2009**, *1161*, 537.
(25) Tagliazucchi, M.; Azzaroni, O.; Szleifer, I. *J. Am. Chem. Soc.* **2010**, *132*, 12404.
(26) Tessier, F.; Slater, G. W. *Macromolecules* **2006**, *38*, 6752.
(27) Tessier, F.; Slater, G. W. *Macromolecules* **2006**, *39*, 1250.
(28) Meller, A. *J. Phys.: Condes. Matter* **2003**, *15*, R581.
(29) Reisner, W.; Morton, K. J.; Riehn, R.; Wang, Y. M.; Yu., Z.; Rosen, M.; Sturm, J. C.; Chou, S. Y.; Frey, E.; Austen, R. H. *Phys. Rev. Lett.* **2005**, *94*, 196101.
(30) Krasilnikov, O. V.; Rodriguez, C. G.; Bezrukhov, S. M. *Phys. Rev. Lett.* **2006**, *97*, 018301.
(31) Klushin, L. I.; Skvortsov, A. M.; Hsu, H.-P.; Binder, K. *Macromolecules* **2008**, *41*, 5890.
(32) Milchev, A.; Klushin, L. I.; Skvortsov, A. M.; Binder, K. *Macromolecules* **2010**, *43*, 6877.
(33) Rafferty, J. L.; Siepmann, J. I.; Schure, M. R. *J. Chromatrogr. A* **2009**, *1216*, 1182.
(34) Boyd, R. H.; Chance, R. R.; Strate, G. V. *Macromolecules* **1996**, *29*, 1182.
(35) Wang, Y.; Teraoka, I.; Hansen, F. Y.; Peters, G. H.; Hassager, O. *Macromolecules* **2010**, *43*, 1651.
(36) Kasianowicz, J. J.; Brandin, E.; Branton, D.; Deamer, D. *Proc. Natl. Acad. U.S.A.* **1996**, *93*, 13770.
(37) Daoud, M.; De Gennes, P. G. *J. Phys. (Paris)* **1977**, *38*, 85.
(38) Kremer, K.; Binder, K. *J. Chem. Phys.* **1984**, *81*, 6381.
(39) Milchev, A.; Paul, W.; Binder, K. *Macromol. Theory Simul.* **1994**, *3*, 305.
(40) Morrison, G.; Thirumalai, D. *J. Chem. Phys.* **2005**, *122*, 194907.
(41) Cifra, P.; Benkova, Z.; Bleha, T. *Faraday Discuss.* **2008**, *139*, 377.
(42) Cifra, P. *J. Chem. Phys.* **2009**, *131*, 224903.

(43) Wang, R.; Virnau, P.; Binder, K. *Macromol. Theory Simul.* **2010**, *19*, 258.
(44) Tegenfeldt, I. O.; Prinz, C.; Cao, H.; Chou, S.; Renner, W. W.; Rieches, R.; Wang, Y. M.; Cox, E. C.; Sturm, J. C.; Silberzan, P.; Austin, R. H. *Proc. Natl. Acad. Sci. U.S.A.* **2004**, *59*, 5833.
(45) MacDowell, L. G.; Müller, M.; Vega, C.; Binder, K. *J. Chem. Phys.* **2000**, *113*, 219.
(46) Müller, M.; MacDowell, L. G. *Macromolecules* **2000**, *33*, 3902.
(47) Kreer, T.; Metzger, S.; Müller, M.; Binder, K. *J. Chem. Phys.* **2004**, 4012.
(48) Landau, D. P.; Binder, K. *A Guide to Monte Carlo Simulation in Statistical Physics*, 3rd ed.; Cambridge Univ. Press: Cambridge, U.K., 2009.
(49) Binder, K., Ed. *Monte Carlo and Molecular Dynamics Simulations in Polymer Science*; Oxford Univ. Press: New York, 1995.
(50) Egorov et al.[20] also did consider an overlap but it was normalized differently. We feel that the present choice is more useful, however. Note also that "densities $\phi_f(r)$, $\phi_g(r)$ in ref 20 already did include the extra factor r, which in eq 4 appears explicitly.
(51) Fleer, G. J.; Stuart, M. A. C.; Scheutjens, J. M. H. M.; Cosgrove, T.; Vincent, B. *Polymers at Interfaces*; Chapman and Hall: London, 1993.
(52) Huinink, H. P.; de Keizer, A.; Leermakers, F. A. M.; Lyklema, J. *Langmuir* **1997**, *13*, 6618.